ELSEVIER

Journal of Chromatography A, 868 (2000) 169–188

JOURNAL OF CHROMATOGRAPHY A

www.elsevier.com/locate/chroma

Optimization of simulated moving bed plants with low efficient stationary phases: separation of fructose and glucose

York A. Beste[a], Mark Lisso[b], Günter Wozny[b], Wolfgang Arlt[a,*]

[a]*Institut fuer Verfahrenstechnik, FG Thermodynamik und therm. Verfahrenstechnik, Building TK 7, TU-Berlin, Straße des 17. Juni 135, D-10623 Berlin, Germany*

[b]*Institut fuer Prozeß- und Anlagendynamik, FG Dynamik und Betrieb technischer Anlagen, KWT 9, Str. des 17. Juni 135, 10623 Berlin, Germany*

Received 2 September 1999; received in revised form 27 October 1999; accepted 28 October 1999

Abstract

An optimization procedure for simulated moving bed (SMB) plants with low efficient stationary phases is presented. The new aspect is that the desorbent consumption can be cut by 70% by running the plant with lower internal liquid flows and a corresponding larger switch time while the productivity is kept constant. This concept was validated by the separation of fructose and glucose in water on a calcium resin with an eight-column SMB plant. The separation can be predicted well by a true moving bed (TMB) and a simulated moving bed simulation. Adsorption isotherms were determined up to 300 kg/m^3 for glucose and 500 kg/m^3 for fructose from 25 to 80°C. Experimental SMB runs were performed over a wide range of feed concentrations (10–350 kg/m^3) and temperatures (25–80°C). The strong influence of the delay volume is pointed out. For an experimental run with high feed concentration a complete set of data is presented. To reduce biological growth separation at 80°C is recommended. © 2000 Elsevier Science B.V. All rights reserved.

Keywords: Simulated moving beds; True moving beds; Fructose; Glucose

1. Introduction

Chromatography is a separation process which uses two auxiliary substances, the stationary and the mobile phase, to separate two or more components. Because these substances can be adjusted to each separation system, chromatography is versatile and can be highly selective: chromatography tends to be more complex but also applicable to difficult separation problems where other separation processes fail. As the demands for purity increase, chromatography gains importance as a unit operation for complex separation problems.

The normal co-current elution chromatography suffers from some disadvantages. It is discontinuous, the products are diluted, and productivity is low which means that only a small amount of product is separated per amount of stationary phase and time. To overcome this, a *simulated* counter-current process, the *simulated* moving bed (SMB), was developed by United Oil Products in 1968. The *true* counter-current process did not succeed because of practical problems. The mechanical stress caused by

*Corresponding author. Tel.: +49-30-314-22775; fax: +49-30-314-22406.

0021-9673/00/$ – see front matter © 2000 Elsevier Science B.V. All rights reserved.
PII: S0021-9673(99)01136-X

the movement of the solid phase tends to destroy it. Additionally a homogeneous and tightly packed bed is needed in chromatography to make a separation possible, especially when the selectivity is low. This quality cannot be reached with a moving solid phase.

In the SMB process the counter-current flow is *simulated* by repeatedly switching the ports of the inlet (feed, make-up) and outlet (extract, raffinate) streams one column in the direction of the liquid flow [1,2].

Because of the complexity of the SMB process and the high number of parameters it is impossible to run a plant by trial and error. Compared to distillation there is no 'total reflux' mode in chromatography, so a thorough investigation before starting the equipment is essential. An optimization procedure is needed to be able to find a set of operating parameters (flow-rates and switch time) which provides the desired separation.

SMB is applied in large scale (sugar and petrochemical applications of up to 10 000 t/year) as well as in small scale applications for valuable products (pharmaceutical, biological, and fine chemical applications of ca. 1–500 kg/year). In recent years the SMB process gained so much confidence that the size of the plants for valuable products is increasing as well. For example, in 1998 UCB, Belgium, successfully installed a plant with six columns (d_C = 450 mm) which produces several tons per year of enantiomer.

There is considerable discussion in literature as to whether elution or SMB chromatography performs better [3–5]. Most authors report that the SMB concept offers higher productivity and lower desorbent consumption. This is certainly true for sugar separation because the resins have a very low efficiency and SMBs do not need high efficient stationary phases compared to batch chromatography. Additionally the amount of product is huge which makes a continuous process especially desirable.

The first part of this paper describes the simulation models (SMB and TMB), the experimental apparatus, and how to determine the necessary model parameters. In Section 4.1 the influence of the delay volume of the plant (e.g. pipes, valves) is pointed out. It is shown that this volume often cannot be neglected [6,7] and how it can be accounted for by the simulation tools. In Sections 4.3 and 4.4 the influence of temperature and concentration are experimentally investigated for the separation of fructose and glucose. Finally in Section 4.5 a simple optimization procedure is described which divides the complex optimization into four comprehensive steps.

2. Theory

This section contains all the equations which are used for the determination of the parameters of the model, for the simulation, and for the optimization. The equations are discussed in more detail in Sections 3 and 4.

2.1. General equations

For the determination of the parameters of the model elution times and variances of experimental peaks and break-through curves have to be determined. This has been done with the method of moments [8]: The equations for the retention time

Table 1
Equations from the method of moments (for symbols see Notation)

	Peak		Front	
t_R	$t_{R,peak} = \frac{\int_0^\infty ct\,dt}{\int_0^\infty} \approx \frac{\sum_{i=1}^n c_i t_i \Delta t_i}{\sum_{i=1}^n c_i \Delta t_i}$	(1)	$t_{R,front} = \frac{\int_0^\infty \frac{\partial c}{\partial t} \cdot t\,dt}{\int_0^\infty \frac{\partial c}{\partial t} \cdot dt} \approx \frac{\sum_{i=1}^n (c^{II} - c_i) \cdot \Delta t_i}{(c^{II} - c^{I})}$	(2)
σ^2	$\sigma^2_{peak} = \frac{\int_0^\infty c \cdot (t - t_R) \cdot dt}{\int_0^\infty c\,dt} \approx \frac{\sum_{i=1}^n c_i (t_i - t_R) \cdot \Delta t_i}{\sum_{i=1}^n c_i \Delta t_i}$	(3)	$\sigma^2_{front} = \frac{\int_0^\infty \frac{\partial c}{\partial t} c \cdot (t - t_R) \cdot dt}{\int_0^\infty \frac{\partial c}{\partial t} \cdot dt} \approx \frac{\sum_{i=1}^n (c^{II} - c_i) \cdot t\,\Delta t_i}{c^{II} - c^{I}}$	(4)

(t_R) and the variance (σ^2) of a peak and a front (=break-through curve) are given in the Table 1. Since the detector signal delivers no continuous curve but discrete points the integrals have to be replaced by sums.

The external porosity (ε_{ext}) can be calculated from the volume of the column, the retention time of a non-adsorbing tracer which cannot penetrate the pores (t_0), and the flow-rate.

The adsorption isotherm was determined by frontal analysis [9]: Assuming a product free initial condition (c^I, $q^I = 0$) the loading of component *i* can be determined from an integral mass balance around the column, Eq. (5), with known flow-rate, volume of the column, retention time of the break-through curve, and equilibrium concentration (c^{II}) after the concentration front.

$$\varepsilon_{ext} V_C \cdot (c_i^{II} - c_i^I) + (1 - \varepsilon_{ext}) \cdot V_C \cdot (q_i^{II} - q_i^I) = \dot{V} \cdot t_R \cdot (c_i^{II} - c_i^I) \quad (5)$$

2.2. Simulation tools

As simulation tools a static TMB model (FORTRAN), a dynamic SMB model (SPEEDUP®), and a dynamic one column model (SPEEDUP) have been used. All models are based on the differential mass balance of a tube reactor with axially dispersed plug flow, linear driving force for the mass transfer, and a non-linear and competitive adsorption isotherm. The known model equations [10,11] are summarized in Table 2.

The **boundary conditions** of Danckwerts (Eqs. (13), (14)) have been used for the TMB model and for the outlet of the SMB model. The outlet condition of Dankwerts sets the concentration gradient to zero at the end of the column. Although very often used this assumption is not very realistic for chromatographic columns. Therefore, the influence of the rear boundary condition is decreased in the more accurate SMB model by always calculating two steps beyond the physical end of the column.

As the **initial condition** for all models all concentrations were set to zero.

The **coefficient of axial dispersion** is assumed to be a linear function of the liquid velocity. Any influence of the molecular diffusion has been neglected because it is small compared to the dispersing effect of the bed for the normal range of flow-rates in liquid chromatography [10, p. 209]. If no adsorption is taking place, the constant of axial dispersion can be determined from the height equivalent to a theoretical plate (HETP) as shown in Eq. (15).

Table 2
Equations of the SMB and TMB models

SMB, one column	TMB
Differential mass balance of the liquid phase	Differential mass balance of the liquid phase
$\frac{\partial c_i}{\partial t} = -w_{liq} \cdot \frac{\partial c_i}{\partial z} + D_{ax} \cdot \frac{\partial^2 c_i}{\partial z^2} - \left(\frac{1-\varepsilon_{ext}}{\varepsilon_{ext}}\right) \cdot k_{eff,solid,i} \cdot (q_i^* - q_i)$ (6)	$0 = -w_{liq} \cdot \frac{dc_i}{dz} + D_{ax} \cdot \frac{d^2 c_i}{dz^2} - \left(\frac{1-\varepsilon_{ext}}{\varepsilon_{ext}}\right) \cdot k_{eff,solid,i} \cdot (q_i^* - q_i)$ (7)
Differential mass balance of the particle	Differential mass balance of the particle
$\frac{\partial q_i}{\partial t} = k_{eff,solid,i} \cdot (q_i^* - q_i)$ (8)	$0 = w_{solid} \cdot \frac{dq_i}{dz} + k_{eff,solid,i} \cdot (q_i^* - q_i)$ (9)
Velocity of the liquid phase	Velocity of the solid phase
$w_{liq} = \frac{\dot{V}}{\varepsilon_{ext} \cdot A_C}$ (10)	$w_{solid} = \frac{L_C}{\tau}$ (11)
Boundary condition at inlet ($z=0$)	Boundary condition at inlet
$c_i^{in} = c_i\big\vert_{z=0}$ (12)	$c_i^{in} = c_i\big\vert_{z=0} - \frac{D_{ax}}{w_{liq}} \cdot \frac{dc_i}{dz}\Big\vert_{z=0}$ (13)
Boundary condition at outlet ($z=L_C$)	Boundary condition at outlet
$\frac{dc_i}{dz}\Big\vert z=L_C$ (14)	$\frac{dc_i}{dz}\Big\vert z=L_C$ (14)

$$C_{D_{ax}} = \frac{D_{ax}}{w_{liq}} = \frac{\text{HETP}}{2} = \frac{1}{2} \cdot \frac{\sigma^2}{t_R^2} \quad (15)$$

For the **adsorption isotherm** the Ching-model [12] was used.

$$q_i^* = K_i c_i + A_i c_i^{(m_i+1)} + B_{ij} c_j^{n_{ij}} c_i \quad (16)$$

This model provides a flexible, binary, non-linear, and competitive description of the thermodynamic equilibrium because it can represent linear, convex and concave isotherms. There is, however, a problem that the first derivative of q_i with respect to c_i or c_j approaches infinity with an exponent between 0 and 1 for concentrations approaching zero.

All **resistance to mass transfer** has been lumped into the linear mass transfer coefficient of the stationary phase. It is assumed to be independent of velocity and concentration.

The **delay volume** (sometimes called extra-column dead volume) of the tubes which connect the columns of the SMB plant is represented in the SMB model by pre-columns in front of every main column. In the pre-column the same tube reactor model, Eq. (6), is used with the porosity set to one and no adsorption taking place. The delay volume cannot be directly modeled in the TMB simulation. To account for it we introduced an effective column length ($L_{C,eff}$) and effective porosity ($\varepsilon_{ext,eff}$). They can be readily calculated from the inner column dead volume ($V_0 = V_C \varepsilon_{ext}$), number and geometry of the columns, and the delay volume (V_{del}) of the connecting tubes. The effective length is the total volume (incl. delay volume) divided by the number (N_C) and cross sectional area (A_C) of columns.

$$L_{C,eff} = \frac{V_{total}}{N_C A_C} = \frac{V_C + V_{del}}{N_C A_C} = L_C + \frac{V_{del}}{N_C A_C} \quad (17)$$

The effective porosity is the volume of the liquid (incl. delay volume) divided by the total volume.

$$\varepsilon_{ext,eff} = \frac{V_{liq}}{V_{total}} = \frac{\varepsilon_{ext} V_C N_C + V_{del}}{V_C N_C + V_{del}} \quad (18)$$

Using these effective values the liquid flow-rate of the TMB process can be calculated from the flow-rate of the SMB with the know relation between SMB and TMB flow-rates [13].

$$\dot{V}_{TMB} = \dot{V}_{SMB} - \frac{\varepsilon_{ext,eff} L_{C,eff} A_C}{\tau} \quad (19)$$

Eqs. (17)–(19) are more thoroughly discussed in Section 4.1.

For **numerical solution** the coupled partial differential equations of the SMB model were transformed with the method of lines [14] into a set of ordinary differential equations. These were solved together with initial and boundary conditions with the commercially available solver SPEEDUP®. Twenty two grid points in the pre-column and 42 in the main column were always used in the SMB simulations.

For the TMB model the method of orthogonal collocation [15] was used to transfer the differential equations and the boundary conditions into a set of non-linear algebraic equations. These were solved numerically with the Newton-Raphson algorithm. Each simulated column contains 10 collocation points. For the solution of simulation problems with high mass transfer and low axial dispersion the number of collocation points can be increased by increasing the amount of simulated columns per real column. In this work the eight real columns were modeled with 24 simulated columns leading to 240 collocation points.

2.3. Parameters characterizing the quality of separation

To be able to compare the quality of separation of several SMBs it is helpful to define the following parameters (e.g. for component A of a binary mixture of A and B in the extract): purity [%]

$$\text{Pu}_{A,E} = \frac{c_{A,E}}{c_{A,E} + c_{B,E}} \cdot 100\% \quad (20)$$

yield [%]

$$\text{Yi}_{A,E} = \frac{C_{A,E} \cdot \dot{E}}{c_{A,F} \cdot \dot{F}} \cdot 100\% \quad (21)$$

productivity [kg/(s.m^3)]

$$\text{Pd}_{A,E} = \frac{c_{A,E} \cdot \dot{E}}{N_C \cdot (1 - \varepsilon_{ext}) \cdot V_C} = \frac{\dot{m}_{A,E}}{V_{solid}} \quad (22)$$

dilution [%]

$$\mathrm{Dl}_{\mathrm{A,E}} = \left(1 - \frac{c_{\mathrm{A,E}}}{c_{\mathrm{A,F}}}\right) \cdot 100\% \quad (23)$$

desorbent consumption [−]

$$\mathrm{Dc} = \frac{\dot{M}}{\dot{F}} \quad (24)$$

Purity and yield characterize the degree of separation. Productivity, dilution, and desorbent consumption describe the efficiency of the separation (e.g. productivity is the mass of product separated with a given amount of stationary phase per unit time). During the optimization of a SMB the parameters purity and yield are improved first. As soon as they are acceptable the quality of separation is improved by increasing productivity and decreasing desorbent consumption.

3. Experimental

3.1. SMB plant

The plant as described by Deckert [16] (Figs. 1 and 2) consists of eight columns C1–C8 ($L_C = 0.499$ m, $d_C = 0.026$ m). To control temperature (design temperature range 25–150°C) the columns were equipped with jackets, heat exchangers HE1–HE8 were added in front of every column, and columns and tubes were insulated with a high temperature resistant polyurethane (Armaflex).

The apparatus is constructed for pressures up to 30 bar. Four membrane-pumps (Lewa) are used to generate feed (PF, 20–200 ml/h), desorbent (PD, 510–5100 ml/h), extract (PE, 170–1700 ml/h), and raffinate (PR, 170–1700 ml/h) streams. The desorbent pump is moved together with the ports every switch time [17]. Thus, it stays always in zone 1, pumps with constant flow-rate, and comes only in contact with pure desorbent. To reach this, two more valves, the cut off valve (VA) and the circuit valve (VK), are necessary per column. To move the streams, four valves (VF, VD, VE, VR) are needed per column so that altogether 48 two-way—valves (Danfoss) are used. Samples can be withdrawn between every column (VPE1 to VPE8) to measure the concentration profile. The make-up[1] stream is continuously degassed with a Teflon-membrane vacuum degasser. Temperature (TIR, PT-100, Conatex) and pressure (PIR, Jumo) are measured for every column. A coriolis mass flow meter (FIR, Rheonik) is located between columns C1 and C2. The extract and raffinate outlet concentrations are monitored online with two UV-detectors (720 LC, Uvicon). The process is controlled by a memory programmable control unit (Simatic S5-115 U, Siemens).

3.2. Determination of the parameters of the model

The experimental system was fructose and glucose (Fluka, purity ≥99%) in de-ionized water. To slightly increase the pH value and prevent corrosion 0.9×10^{-3} kg/m^3 Na_2CO_3 was added to the water. All columns were slurry packed with the Ca-resin Lewatit MIDS 1368 (cross-linked copolymer of polystyrene and divinylbenzene, d_p (90%) = 350±50 μm) which was supplied by Bayer AG. The experiments were carried out at constant temperatures between 25 and 80°C and a back pressure of 5 bar. The pressure drop was approximately 0.1 bar per column.

The **parameters of construction** are $N_C = 8$, $d_C = 0.026$ m and $L_C = 0.499$ m.

The **delay volumes** (Table 3) of tubes, valves, heat exchangers, flow meter, and pumps were determined from the elution time of a tracer with the columns removed. The total delay volume sums to 92.18×10^{-6} m^3 which is approximately 4% of the total volume.

The physico-chemical parameters are (external) porosity, adsorption isotherms, coefficients of axial dispersion, and mass transfer.

The mean **porosity** ($\varepsilon_{ext} = 0.389$) was measured with blue Dextran (Fluka, MI = 2×10 kg/kmol, purity ≥99%). No column porosity differed more than ±0.005 from this value.

The **adsorption isotherms** were determined by frontal analysis between 25 and 80°C. The retention times of the break-through curves were corrected for the delay time, which was measured from a break-through curve with the column removed from the

[1] For an explanation of the make-up stream see Fig. 4a.

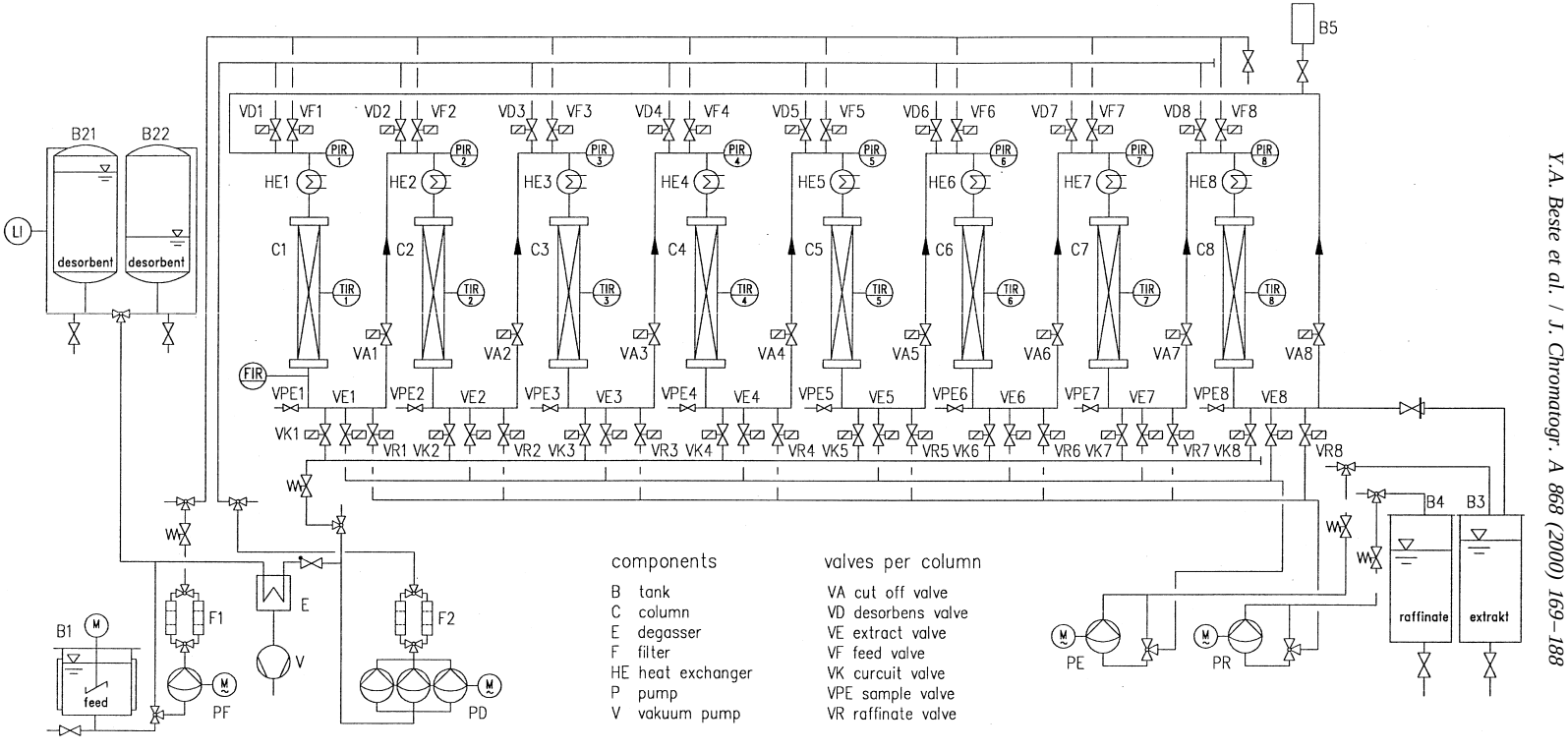

Fig. 1. Circuit diagram of the simulated moving bed plant.

Fig. 2. Photo of the SMB plant (without insulation).

system. All thermodynamic measurements were performed on a binary high pressure gradient HPLC (HP 1100, online degasser, binary pump, auto sampler, column compartment, DAD-detector). The loading (q_i) was calculated with Eq. (5). Finally the parameters of the Ching model were fitted by non-linear regression to the adsorption data. The isotherms of the pure components were investigated up to 500 kg/m^3 for fructose and 300 kg/m^3 for glucose.

The competitive adsorption data were determined by frontal analysis as well. It was not possible to use the perturbation method because the broad peaks overlapped significantly. SMB experiments with the same flow-rates but different feed concentrations showed that the profile of fructose, in contrast to glucose, did not change. From this behavior it can be concluded that the adsorption of fructose is linear and not influenced by glucose. Therefore the breakthrough curves of glucose could be investigated with a constant background concentration of fructose (100, 200, and 300 kg/m^3). A differential refractive index detector (Knauer) was added because a UV-detector cannot visualize glucose if fructose is present. Unfortunately the signal of the refractive detector was very non-linear due to the fructose concentration (no polarity meter was available). Therefore the competitive isotherm could only be determined for low concentrations of glucose (0–8 kg/m^3). The competitive parameter B_{GF} was determined for $T=25$°C by non-linear regression of the data in Table 4 keeping the pure component parameters (K_i) of the isotherm constant. In view of the good agreement for 25°C (see Fig. 5) the value of B_{GF} (80°C) was fitted directly to the experimental data of a high concentrated SMB run ($c_F^{feed}=281$

Table 3
Delay volumes between columns of the SMB plant

Between columns	8→1	1→2	2→3	3→4	4→5	5→6	6→7	7→8
V_{del} [10^{-6} m^3]	17.65	13.68	10.54	9.41	10.23	9.88	10.73	10.06

Table 4
Competitive adsorption data for 25°C, gray squares: $q_G = f(c_G, c_F)$

c_F [kg/m^3] → / c_G [kg/m^3] ↓	100	200	300
0	0	0	0
4	1.361	1.534	1.784
8	2.606	2.996	3.487

kg/m^3, $c_G^{feed} = 244$ kg/m^3, 80°C). For 40 and 60°C the SMB feed concentrations were too low to observe any interactions.

Table 5 lists the resulting parameters of the Ching adsorption isotherm, Eq. (16) and the selectivity (α_{FG}) for the investigated temperatures. The pure components show a linear behavior. The glucose leaves the linear region as soon as a higher concentration of fructose is present. Therefore a linear model is not sufficient to describe the behavior of glucose.

For all temperatures for which parameters are not listed in Table 5 the following constant values have been used: $A_F = A_G = 0$, $m_F = m_G = 0$, $B_{FG} = 0$, $n_{FG} = n_{GF} = 1$.

The constant of **axial dispersion** ($C_{D_{ax}}$) was calculated from Eq. (15) from a peak of blue Dextran. The resulting axial dispersion (D_{ax}) (Table 6) corresponds well with a correlation from Butt [18]. An additional comparison of the experimental and simulated peaks calculated with the one column model also showed good agreement. Since the coefficient of axial dispersion has a very small effect on the simulations, the value of room temperature was used for all temperatures.

The **mass transfer coefficients** ($k_{eff,solid}$) (Table 6) were determined by fitting simulated (one column model) to experimental break-through curves for fructose and glucose. This procedure can be explained with Fig. 3 which compares several simulated break-through curves with different $k_{eff,solid}$ to an experimental curve. As expected the break-through curves become sharper with increasing mass transfer coefficient. The retention times calculated from Eq. (2) are independent of the mass transfer. This represents the experimental behavior well because the retention time of a break-through curve depends only on the thermodynamic equilibrium. For the temperature of 40°C the smallest deviation between calculation and experiment is reached between the curves of $k_{eff,solid} = 0.015$ l/s and $k_{eff,solid} = 0.010$ l/s. The exact fit has been carried out separately for the two components at every temperature. The closest calculated curve still cannot exactly predict the slow approach to the final concentration of the experimental curve, as shown in Fig. 3. The agreement, however, is considered to be sufficient.

Table 5
Parameters of the Ching isotherm and selectivity in the linear case

T [°C]	K_F [−]	K_G [−]	B_{GF} [−]	α_{FG} [−]
25	0.675	0.32	0.000457	2.11
40	0.610	0.32	0[a]	1.91
60	0.541	0.324	0[a]	1.67
80	0.610	0.368	0.00028	1.66

[a] Competitive adsorption data have only been investigated for temperatures of 25 and 80°C.

3.3. Experimental runs

Runs at 25, 40, 60 and 80°C were performed to investigate the influence of temperature on the separation. The concentration was increased from 10

Table 6
Constant of axial dispersion (Eqs. (15)) and coefficient of mass transfer (Eqs. (8) and (9)) as a function of temperature

T [°C]	$C_{D_{ax}}$ [m]	$k_{eff,solid,F}$ [l/s]	$k_{eff,solid,G}$ [l/s]
25	0.00153	0.012	0.015
40	0.00153	0.013	0.018
60	0.00153	0.015	0.019
80	0.00153	0.015	0.019

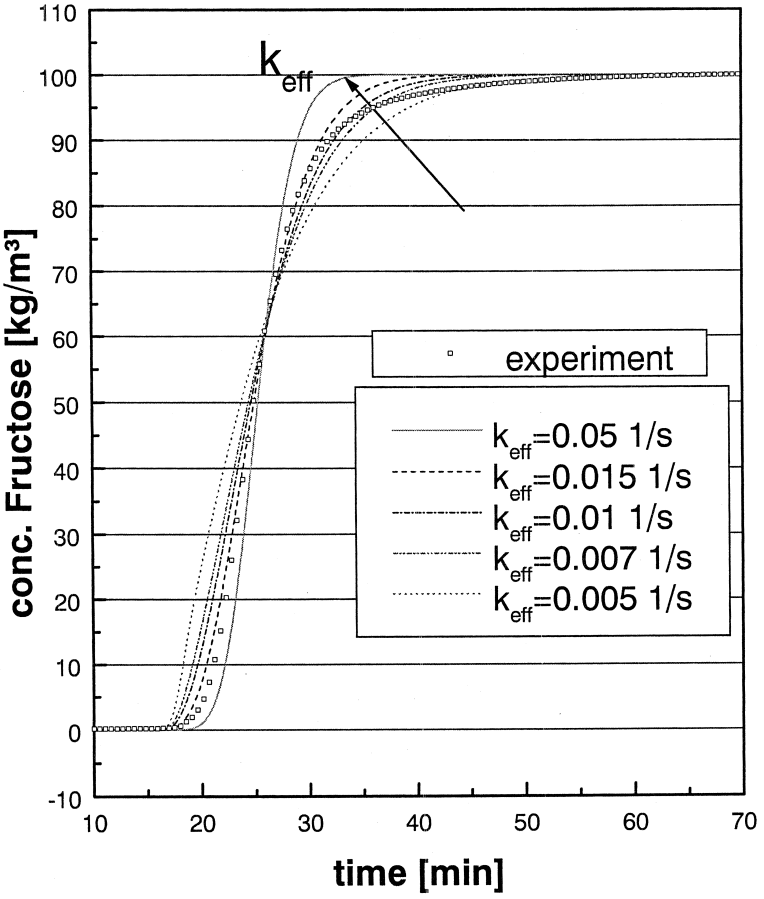

Fig. 3. Comparison of simulated and measured break-through curves at 40°C.

to ca. 350 kg/m^3 to see the effect of competition between fructose and glucose. Finally the internal flow-rate/switch-time relation was varied to decrease dilution and desorbent consumption. Altogether more than 25 runs lasting from 16 h to several days were performed. To compare experimental runs with simulations, samples were drawn from the sample valves between every column in the middle of a switch time and from feed and product streams continuously. The concentrations were analyzed with the same HPLC as used for frontal analysis. For the solvent ACN–water (75:25 vol.-%) and for the stationary phase NH_2-covered silica gel were used. The accuracy of the analysis was 1.5% for higher concentrations ($c \geq 10$ kg/m^3) and 5–10% for small concentrations ($c \leq 1$ kg/m^3).

4. Results and discussion

4.1. Effect of connecting tubes (delay volumes)

In Fig. 4 the concentration of fructose and glucose is shown over the 8 columns of the SMB plant at half switch time. The liquid is flowing from left to right and the simulated solid flow moves counter-currently from right to left. fructose, which is the stronger adsorbing component, moves preferentially with the stationary phase to the left, while glucose moves to the right. In addition to the experimental data two SMB simulations are shown. The thick black lines take into account the influence of the delay volumes of the valves and tubes between the columns by simulating pre-columns. The volume of

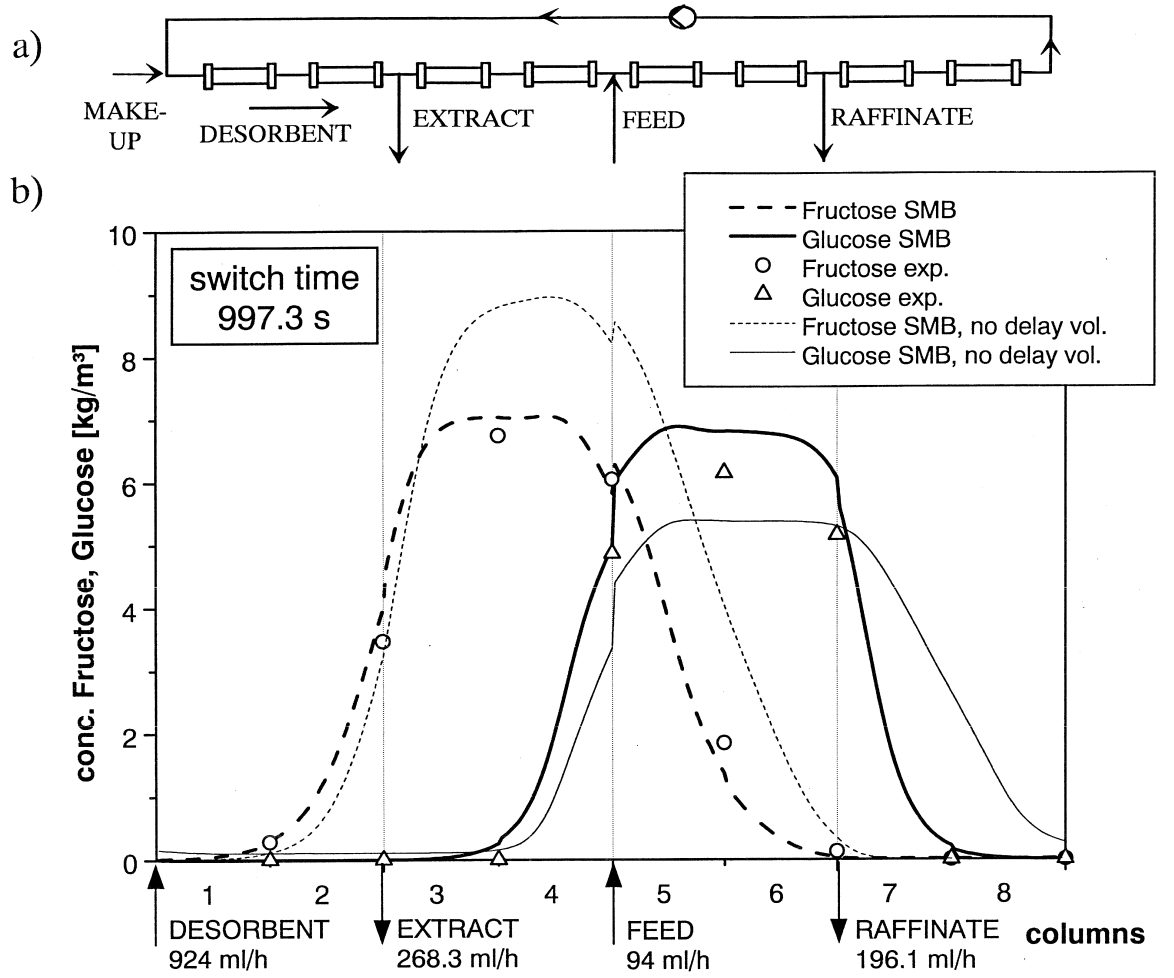

Fig. 4. (a) Sketch of the configuration of columns of the SMB with names of streams. (b) Comparison of experimental data with simulations with and without the delay volumes (SMB).

the pre-columns correspond with the measured delay volumes. All simulations use the independently determined adsorption isotherms. Neglecting the delay volume (thin lines), which represents only 4% of the total volume, leads to a strong deviation from the experimental result. fructose and glucose are shifted to the right. Thus, the raffinate outlet is contaminated with fructose and glucose breaks through at the end of column 8. The concentration of the plateau around the feed port of fructose is higher while the plateau of glucose is lower. These effects can be explained by looking at the product ports. The concentration of fructose around the extract port is decreased by the shift to the right. Thus, less fructose leaves the plant via the extract port and the concentration in the quasi-steady state is higher. The opposite is true for glucose. Its concentration at the raffinate port is higher, so more leaves the apparatus and the hold up concentration is decreased. Introducing the delay volumes in the simulation has the same effect as decreasing the desorbent flow-rate. This is reasonable because the liquid needs time to move through the additional volume.

In the SMB simulation the delay volumes can be modeled in a straight forward way by precolumns. Simulation results show that the right description of the delay time is much more important than the additional axial dispersion in the delay volume itself

[7]. Therefore, the value of $C_{D_{ax}}$ in the pre-column can be the same as in the main column unless some physical components, which lead to additional dispersion, are introduced into the plant.

Eqs. (17)–(19) describe a simple way to take into account the delay volume in a TMB simulation. Because pre-columns cannot be simulated here, the delay volume is expressed by an effective length and porosity. A different formulation of this approach has been proposed recently [6] and discussed in detail [7]. A closer look reveals that the different approaches lead to the same results. We prefer this approach because only the effective length and porosity have to be calculated. All the other equations (working triangle, TMB model) which were valid ignoring the delay volume do not have to be changed. The good agreement between SMB and the 'corrected' TMB simulations (see Fig. 5) prove the feasibility of this approach. If physical meaningful parameters are to be used in the calculation the strong influence of the delay volume must be taken into account.

4.2. Validation of the programs

The simulation programs were validated by comparing calculated and experimental results. Fig. 5 compares TMB and SMB simulations with experimental results in the middle of the first period of the 10th cycle. Both calculations predict the experimental concentrations very well. SMB and TMB calculations are in a good agreement also. The TMB simulation predicts unrealistic profiles around the feed port. This disadvantage is not significant: the important concentrations around the two product ports are represented well.

Table 7 contains experimental and simulated parameters characterizing the quality of separation.

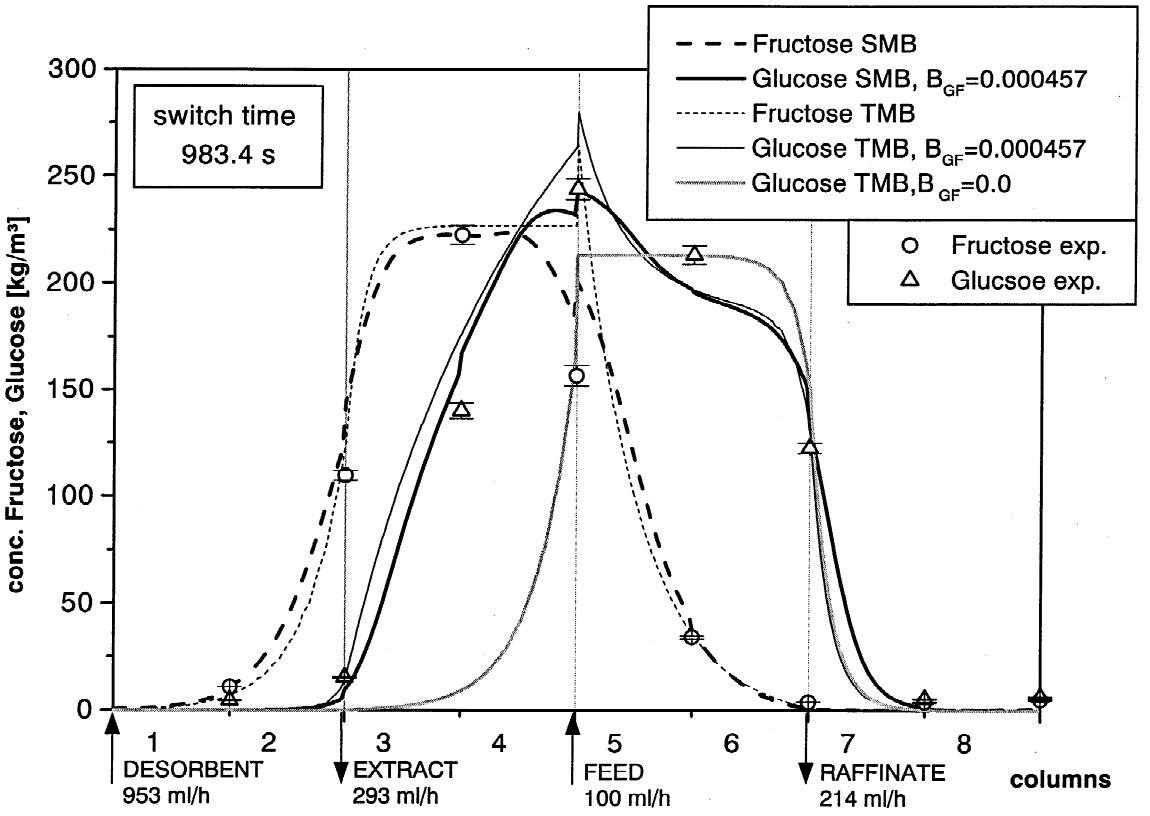

Fig. 5. Comparison of experimental and simulated results for a highly concentrated SMB run $c_F^{Feed}=363$ kg/m^3, $c_G^{Feed}=322$ kg/m^3.

Table 7
Calculated and experimental parameters characterizing the quality of separation in Fig. 5

		TMB	SMB	exp.
Purity	Extr.	90.4	89.4	81.6
[%]	Raff.	99.0	97.9	92.9
Yield	Extr.	99.0	98.3	96.4
[%]	Raff.	88.1	86.9	80.4
Productivity	Extr.	7.7	7.7	7.5
[10^{-3} kg/sm^3]	Raff.	6.1	6.0	5.6
Dilution	Extr.	66.2	66.4	67.1
[%]	Raff.	58.8	59.4	62.4

The experimental results show that the columns of the SMB are too short to reach a total separation for the given feed flow-rate. The difference between predicted and measured purities can be explained by the steep profiles at the product ports. Small deviations lead to large errors. The TMB simulation always calculates values which are too optimistic. This is true in general if TMB and SMB simulation results are compared and has to be kept in mind when a TMB model is used. On the other hand the simulation time needed to reach the pseudo steady state is less than 1 min for the TMB (Pentium 100 MHz) and approximately 4–5 h for the SMB model (Sun Ultra Spark I). Additionally the concentration profiles at half switch time are nearly identical to the SMB profiles. This shows that the TMB program gives a fast and reasonably accurate estimate of the real behavior. The calculation speed makes it suitable for repeated runs during the optimization of SMB processes (see Section 4.5).

Fig. 6 shows the signal of a UV-detector at the extract outlet during the start up period of an SMB run (c_F^{Feed}, $c_G^{Feed} = 50$ kg/m^3) as a function of time. It elucidates the periodic character of simulated moving bed chromatography. The saw-blade type curve starts at zero concentration and approaches the pseudo-steady state after approximately 450 min (see Fig. 7). The experimental data are compared to the SMB simulation. Every switch period both curves perform a sharp increase followed by a smoother decrease.

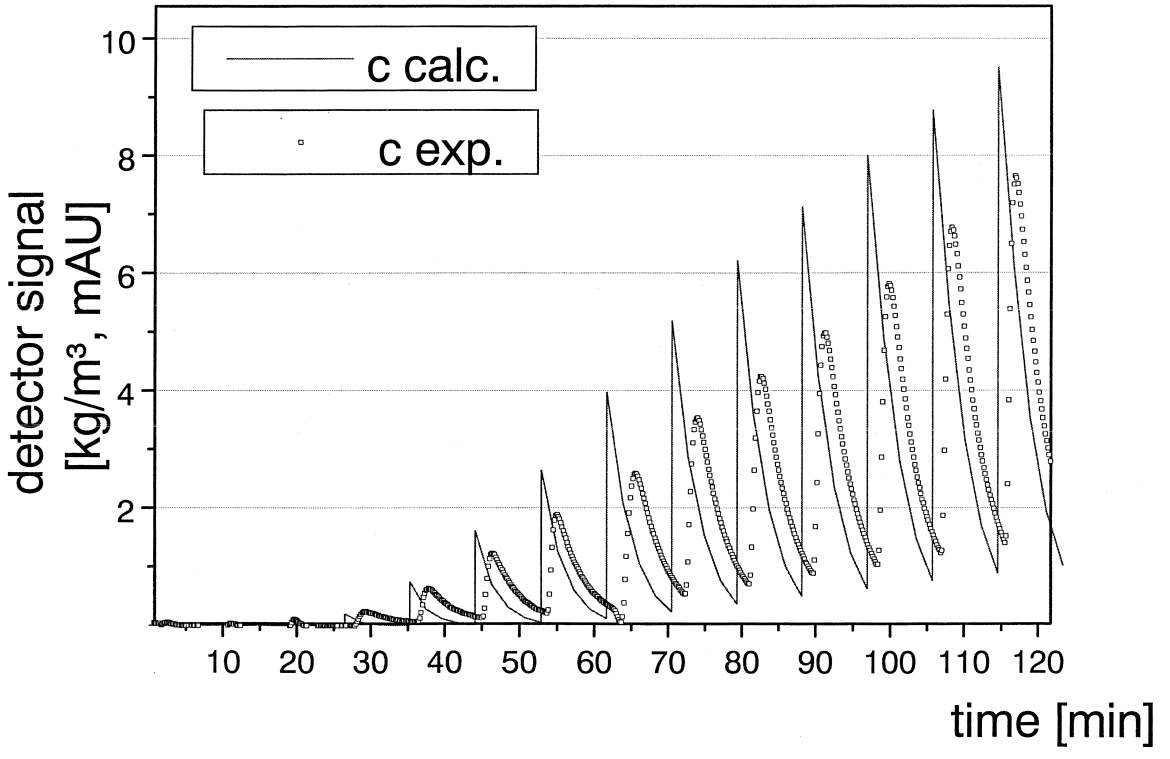

Fig. 6. Comparison of experimental and simulated results at the extract port in the start-up period.

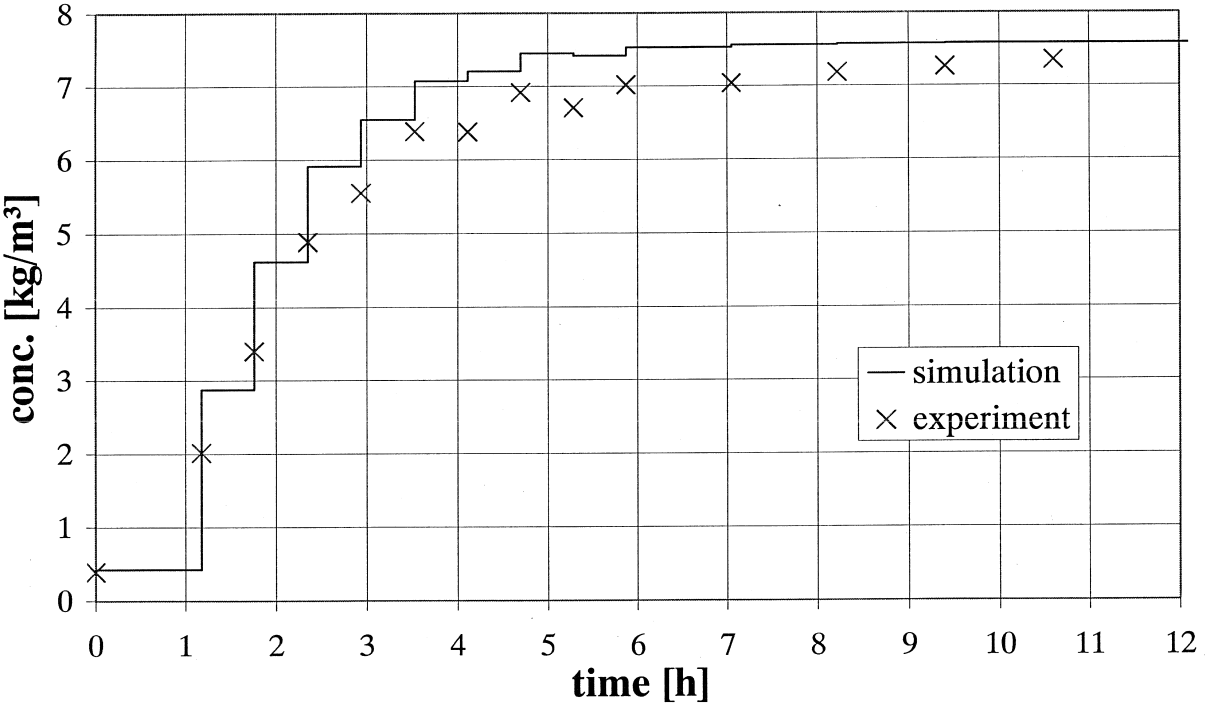

Fig. 7. Comparison of averaged experimental and simulated concentrations at the extract port.

This form is typical for the extract port. In the beginning of a switch period the extract concentration is high because the profile in Fig. 4 starts shifted half a column to the left side. During the period the concentration profile moves to the right and the concentration of the extract slowly decreases to the minimum just before the next switch. After the switch it jumps back to the high concentration. The profile of the raffinate port has a saw-blade type curve as well but with a slow decrease followed by a sharp increase in concentration in every switch period.

The experimental curves are smoother and always lag behind the simulations. This is because the extract pump with its connecting tubes are located between the columns and the detector. Since it is not essential for the separation performance the mixing effect of the product pump and the time delay of the outlet tubes have not been accounted for in the simulation. The delay times calculated from the volume of the tubes and the extract flow-rate fit exactly to the delay times of Fig. 6. (Note that the delay volume is different for every column because of the asymmetry of the plant. Thus, the simulated curve cannot be shifted as a whole to the right.)

In Fig. 7 the averaged concentrations of simulation and experiment at the extract port are compared. The simulation reaches the quasi steady state at approximately 6 h which is about 2 h faster than the experimental values. Nevertheless the agreement is good.

4.3. Effect of temperature

Performing a separation at a higher temperature is of interest to the food industry in order to prevent biological growth. Additional positive effects are the decreased viscosity, and corresponding decreased pressure drop, and an increased solubility of the components in the solvent.

The measured parameters show that a change of temperature affects the thermodynamics and the mass transfer. Porosity and axial dispersion stay constant. The equilibrium constant of glucose increases with temperature while the equilibrium constant of fructose decreases clearly up to 60°C and

than increases again for 80°C (Table 5). The selectivity steadily decreases, the influence of interaction decreases (B_{GF}), and the mass transfer coefficients of both components steadily increase with temperature. No degradation of the stationary phase (Lewatit) was observed at any temperature. This was proved by analyzing the water content of the resin which gives information about the degree of cross-linking. It stayed constant even if the Lewatit was stored at 120°C for several days. No degradation of the carbohydrates could be observed either. The SMB experiments (not shown[2]) agree well with the simulations. The efficiency of the system could be increased from a NTU of 195 to 237 calculated for glucose with a flow-rate of 500 ml/h. This positive effect was more than compensated by the decrease in selectivity. Thus, the purity of the products decreased about 7% while the productivity was kept constant.

These results show that by paying attention to the changing adsorption isotherms the separation can be carried out at higher temperatures, therefore making use of the advantages mentioned above. The decrease in selectivity can be compensated for by increasing the length or the number of columns of the SMB. Since the stationary phases commonly used in sugar separation are relatively cheap the additional cost will not be high.

4.4. Effect of high concentration

To explain the effect of high concentration a calculation neglecting the interactions ($B_{GF}=0$, only glucose) is included in Fig. 5 (thick gray line). This profile fits well to the experimental data points in the regions where fructose is not present (e.g. columns 5–8). A serious deviation from the experimental values can be found in columns 2–4. This is the region where glucose and a high concentration of fructose are present, thus the region of interaction. Using the parameter BOF, determined from independent frontal analysis measurements, leads to a good prediction of the experimental concentrations at the end of columns 2–4. The concentrations in columns 5 and 6 change as well but still represent the experimental data well. The fact that the curves for fructose (dashed lines) agree well with the experimental results shows that fructose is not influenced by glucose.

It can be concluded that neglecting the interaction leads to an impure extract at high concentrations because the selectivity seriously decreases. Complete separation can be reached if section II is optimized by increasing $\dot{V}_{II}$ (see section 4.5) which would lead to a smaller productivity.

4.5. Optimization procedure

Following the procedure described in this section suitable operating parameters (feed, desorbent, extract, raffinate flow-rates, and switch time) can be derived for a given SMB plant if the parameters of the model are known. The procedure is structured into four steps (Fig. 8). During the entire optimization procedure two constrains have to be kept in mind. First the feed concentration is limited by the solubility of the components in the eluent and second the maximum flow-rate is given by the maximum pressure drop. To estimate the pressure drop, the Kozeny-Carman equation [13] or the VDI-Wärmeatlas [19] can be used.

In the **first step** a starting set of operating parameters is generated. For this only the constructive parameters, the porosity and the thermodynamic conditions (isotherms) have to be known. Mass transfer and axial dispersion are neglected (ideal chromatography). For a system with linear isotherms the operating parameters can be calculated immediately if the flow-rate of the feed and a stability factor are specified by the user [1]. If the isotherms are not linear but can be described by a Langmuir, a modified Langmuir, or a bi-Langmuir model the working triangle method [20,21] can be used to take into account the concentration of the feed. This method is based on the theory of multi component chromatography [22,23]. It results in equations which explicitly describe the region of total separation. The operating parameters including the feed concentration can be chosen to reach a point of operation which lies in this region. This method is an efficient and powerful tool for highly efficient stationary phases ($d_p \leq 20$ μm) where mass transfer is fast enough to be neglected.

In cases where the effects of mass transfer and

[2]Data can be obtained from the authors.

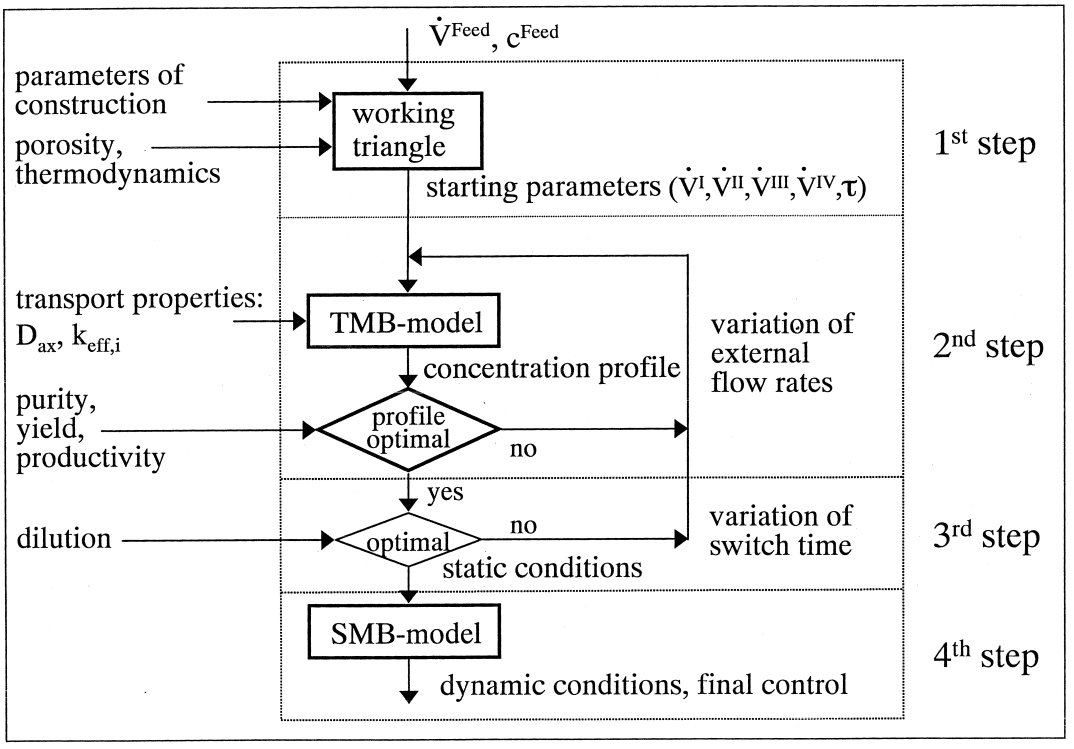

Fig. 8. Optimization procedure.

dispersion cannot be neglected and the isotherm is not linear and not of the Langmuir type the first step of the optimization should take into account only the linear part of the isotherms to generate starting values, and the optimization should continue directly with the second step.

In the **second step** [24] the concentration profiles are calculated with the TMB model. For this the operating parameters of the first step are used and the transport properties (axial dispersion and mass transfer) have to be known. Note that here and in the first step, so always when TMB simulation is applied, the effective porosity and column length should be used.

To optimize the entire SMB the four sections are investigated separately. Every section has a special task to fulfill. In section I between the desorbent and the extract port the stationary phase of column 1 has to be fully desorbed before it is shifted to section IV. In section IV between the raffinate and the desorbent port the solvent has to be cleaned before it is recycled to section I. In sections II and III the separation of the components takes place.

Fig. 9 shows the concentration profile calculated with the starting parameter generated in step one as thin black lines at half switch time. Because the SMB behavior equals the TMB simulation only in the middle of the switch period, the concentration profiles in the real SMB process are located in the beginning of a switch period half a column to the left and at the end half a column to the right. To prevent component A or B from being shifted with column 1 from section I into section IV at the end of a period the concentrations have to be zero in the entire column. This condition is equal to the concentration being zero in the middle of column 1 at the half switch time (see the solid triangle in column 1 at the abscissa of Fig. 9). The second half of the period is then used to flush component A out of the right half of column 1. Because of this difference between the SMB and the TMB process all borders of optimization are moved as indicated by the triangles in column 1, 3, 6 and 8.

The thin concentration curve in Fig. 9 does not fulfill the requested desorption in section I. To

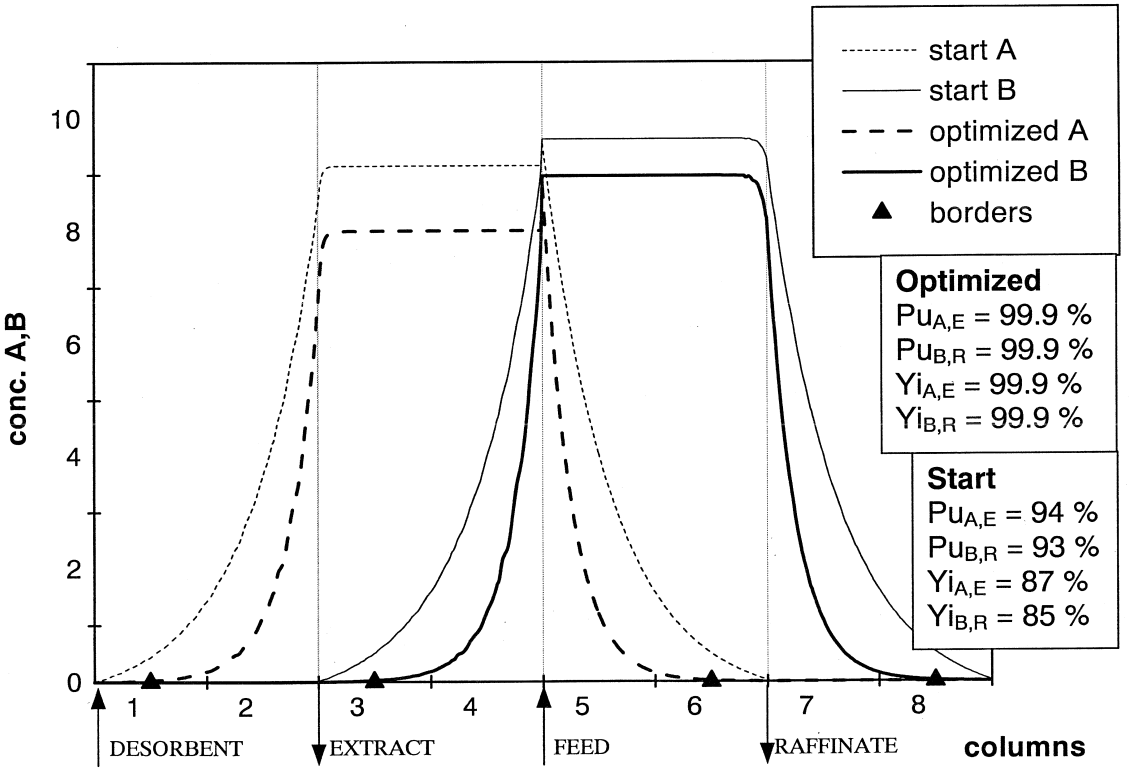

Fig. 9. Initial and final result after optimization of all sections with the TMB model.

optimize this section without changing the situation in other sections its internal flow-rate has to be increased. This can be done by increasing the desorbent and extract flow-rates by the same amount leaving all other parameters constant. The value of the internal flow-rate is optimal if the concentration of A reaches zero at the solid triangle. Next, section IV is optimized by decreasing the internal flow-rate until the concentration of component B has reached zero at the solid triangle in the middle of column 8. Section II follows where component B has to reach zero in the middle of column 3 and section III where component A has to reach zero in the middle of colunm 6. In Fig. 9 the final concentration profile can be seen as thick black lines. Extract and raffinate consist nearly of 100% A or B respectively. For the optimization of sections II and III the feed flow-rate must be decreased which leads to a decrease in concentration and thus in productivity. This effect, that the purity can only be increased at the cost of productivity, is the typical behavior of separation processes.

The second step of the optimization procedure including the consequences for the process is summarized in Table 8.

In the **third step** the liquid flow-rate/switch time relation is optimized. So far the switch time has been kept constant. To keep the migration velocity of the substances constant the switch time has to be increased if the liquid flow-rate is decreased and vice versa. Note that for a SMB it is possible to chose the inner flow-rates in a certain range independently of the external flows. Therefore several 'optimized' states of a SMB with different switch times are possible and the best one has to be found.

The van Deemter curve [9] shows that the NTU decreases with increasing flow-rate. Thus, the aim is to find the minimal possible internal flow-rate with the appropriate switch time which fulfills the specified separation problem (c_F and $\dot{F}$). This is done

Table 8
Optimizing the four sections of a SMB

Aim	Change of internal flow-rate	Change of external flow-rate	Consequences for the process
Complete desorption of recycled solid phase	Increase $\dot{V}_{I}$	1. Increase make-up 2. Increase extract	Dilution of extract
Complete cleaning of recycled liquid phase	Decrease $\dot{V}_{IV}$	1. Increase make-up 2. Increase raffinate	Dilution of raffinate
Increasing purity of extract	Increase $\dot{V}_{II}$	1. Decrease feed 2. Decrease extract	Decrease of productivity
Increasing purity of raffinate	Decrease $\dot{V}_{III}$	1. Decrease feed 2. Decrease raffinate	Decrease of productivity

by multiplying the switch time with and dividing the desorbent flow by the same factor, then optimizing the concentration profiles with the TMB model (step 2) keeping the feed flow-rate constant, and finally comparing the sets of parameters with respect to purity, yield, productivity and desorbent consumption. This optimization is limited by the lowest internal flow-rate which leads to the requested purities for the given feed.

In Fig. 10 two SMB runs with different switch

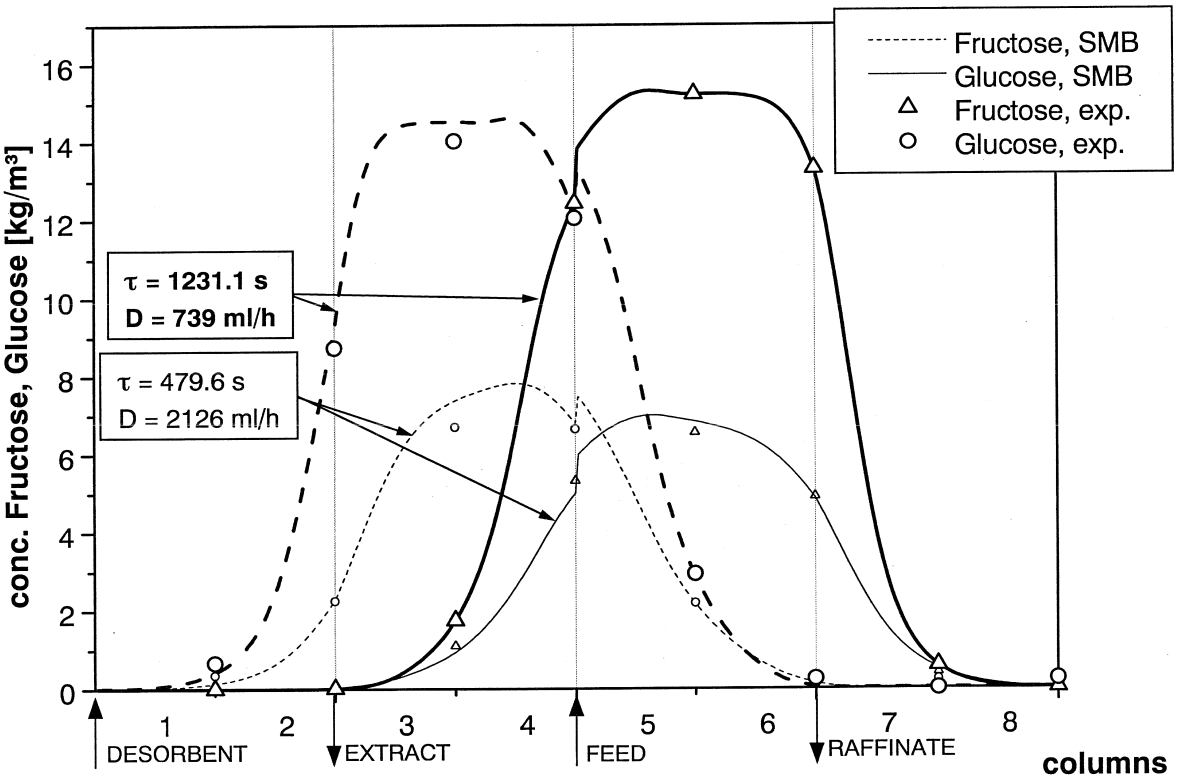

Fig. 10. Comparison of SMB runs with low and high switch times.

times but equal feed flow-rates are compared. The concentration profile with the high switch time and the low desorbent flow-rate is a lot sharper which equals a higher NTU. Thus, the inner concentration around the feed port can be increased without a loss in purity which leads to a higher concentration of the products and a 70% reduced desorbent consumption (Table 9). To check these results simulations with a doubled column length ($L_C = 0.998$ m) have been carried out. They showed exactly the same behavior.

This optimization of the switch time affects only mass transfer controlled processes, where the HETP increases with the velocity. This is true for most of the cases in chromatography, but the effect is less significant as the mass transfer resistance decreases. For high-performance stationary phases ($d_p \leq 20$ μm) the effect will have only a minor influence.

Unfortunately the time to reach pseudo-steady state is increased by a higher switch time. For the separation of fructose and glucose 8 to 9 cycles were always needed to reach steady state independent of the switch time. Because the switch time of the optimized run is 2.5 times higher, the start-up time will be 2.5 times higher also. In this case time can be saved by starting with a fast switch time and jumping to a slow one when the steady state comes closer (e.g. third to fourth cycle).

Finally in the **fourth step** the TMB results are checked with the SMB program because it is much closer to reality. The product concentrations and the parameters characterizing the quality of separation are take from the SMB simulation. Additional results are the start up time and the dynamic behavior of the apparatus.

In this optimization procedure the TMB model, a fast and acceptably accurate simulation tool, does most of the work. The SMB model is only used for controlling and fine tuning purposes because of the long calculation times. Some authors state that the simulation of concentration profiles with TMB models is redundant because they do not give more information than the working triangle method, which is the first step of the above proposed optimization procedure and is based on the true moving bed also. We think this is not true. With the concentration profiles the borders of optimization can be moved to the middle of the columns as shown in Fig. 9. Thus, a lot of the differences between the SMB and TMB simulations are compensated. The result is the much shorter simulation time of the TMB model which makes it perfectly suitable for the repeated runs in optimization procedures.

After optimizing a stand-alone SMB plant, the next aim is to optimize the complete process in which the SMB represents only one unit operation. This can be done with the TMB model which has been implemented as a user-added module[3] into the flow-sheeting program CHEMICAD®. This tool makes fast cost estimation possible and helps in the synthesis of processes.

Table 9
Parameters characterizing the quality of separation in Fig. 9

	$\tau = 479.6$ s	$\tau = 1231.1$ s
Purity (%)	97.9	99.7
Yield (%)	97.9	99.7
Dilution (%)	81	48
Make-up (ml/h)	980	294
Desorbent consumption	9.8	2.9

5. Conclusion

An SMB and a stationary TMB simulation program have been validated with experimental data over a wide range of concentrations and temperatures for an eight column SMB plant. The TMB program represents the SMB behavior well.

The strong influence of the delay volume on the simulation results has been shown. To calculate with physical meaningful parameters the delay volume has to be taken into account. Thus, pre-columns were implemented in the SMB model. For the TMB model a procedure has been introduced to represent the influence of the delay volume by an effective porosity and column length. Equations are given to directly calculate these effective values from the delay volume. This leads to good agreement with the experimental data, and thus, the benefit of the short simulation times of the TMB model can be obtained.

[3] Available from the authors.

The SMB plant performed well up to a temperature of 80°C. At the high temperature biological growth can be prevented or at least slowed down which leads to less cleaning breaks for continuous producing plants. Additional positive effects of the high temperature are the higher solubility, the lower viscosity, and the lower pressure loss. The resin was stable up to 120°C. Therefore, the separation at 80°C is recommended.

At higher concentration the adsorption of glucose is increased by the presence of fructose while the adsorption of fructose behaves linearly in the investigated range up to 500 kg/m^3 and is not influenced by glucose. This behavior can be described well using the parameter B_{GF} of the Ching isotherm. If this interaction is not taken into account the extract will be contaminated with glucose.

An optimization procedure has been described. Besides the working triangle method it makes use of a TMB and a SMB model. Because of the short calculation times the use of TMB is recommend for repeated runs in the optimization procedure. Special care was taken to optimize the liquid flow-rate/switch time relation. The inner flow-rates of the SMB can be chosen in a certain range independent of the external flows. Because a small liquid velocity leads to a small HETP and therefore to a higher efficiency of the apparatus, it is recommended to run SMBs which contain low efficient stationary phases with the smallest internal flow that is possible. Thus the desorbent consumption could be decreased by 70% while purity, yield, and productivity were kept constant.

6. Notation

A, B	parameters of the ching isotherm (−)
A_C	cross sectional area of column (m^2)
c	concentration in the liquid phase (kg/m^3)
$c_{D_{ax}}$	parameter of the coefficient of axial dispersion
Dc	desorbent consumption (−)
d_C	diameter of column (m)
$\dot{D}$	flow-rate of desorbent, flow-rate in section I (ml/h)
Dl	dilution (%)
D_{ax}	coefficient of axial dispersion (m^2/s)
$\dot{E}$	flow-rate of extract (ml/h)
$\dot{F}$	flow-rate of feed (ml/h)
HETP	height equivalent of a theoretical plate (m)
$k_{eff,solid}$	linearised coefficient of mass transfer in the solid phase (l/s)
K	equilibrium constant, (−)
L_C	length of column (m)
$\dot{M}$	flow-rate of make-up stream (ml/h)
N_C	number of columns (−)
m,n	exponents of the Ching isotherm (−)
Pd	productivity (kg/sm^3)
Pu	purity (%)
q	loading, concentration of the stationary phase (kg/m^3)
$\dot{R}$	flow-rate of raffinate (ml/h)
t_R	retention time (min)
$\dot{V}$	flow-rate of the liquid phase (ml/h)
V_C	inner volume of the column (m^3)
V_{del}	delay volume between columns (m^3)
Yi	yield (%)

Greek symbols

ε_{ext}	external porosity (−)
$\varepsilon_{ext,eff}$	effective ext. porosity (to account for V_{del})
σ	variance (s^2)
τ	switch time (s)

Superscript

I, II	before, after the concentration step (FA)
*	in equilibrium

Subscript

A	stronger absorbing component
B	weaker adsorbing component
C	column
E	extract
F	fructose
G	glucose
i, j	component i, j
liq	liquid
R	raffinate
rel	relative
solid	solid
I, II, III, IV	section of the TMB or SMB

References

[1] D.M. Ruthven, C.B. Ching, Chem. Eng. Sci. 44 (1989) 1011.
[2] P. Deckert, W. Arlt, Chem. Ing.-Tech. 66 (1994) 1334.
[3] R.M. Nicoud, M. Bailly, Proceedings of Prep 92, 1992
[4] C. Heuer, H. Kniep, T. Falk, A. Seidel-Morgenstern, Chem. Ing. Tech. 69 (1997) 1535.
[5] P. Jusforgues, M.I. Shaimi, H. Colin, D. Colopi, Proceedings of SPICA 98, Strasbourg, 1998
[6] H. Kniep, Ph.D. Thesis, Otto-von-Guericke-Universität Magdeburg, 1998, p. 100
[7] C. Migliorini, M. Mazzotti, M. Morbidelli, AIChE J. 45 (1999) 1411.
[8] K.-H. Radeke, Chem. Ing. Tech. 34 (1982) 401.
[9] G. Guiochon, S. Golshan Shirazi, A.M. Katti, Fundamentals of Preparative and Nonlinear Chromatography, Academic, Boston, 1994.
[10] D.M. Ruthven, Principles of Adsorption and Adsorption Processes, John Wiley, New York, 1984.
[11] L.S. Pais, J.M. Loureiro, A.E. Rodrigues, AIChE J. 44 (1999) 561.
[12] C.B. Ching, K.H. Chu, D.M. Ruthven, AIChE J. 36 (1990) 275.
[13] F. Charton, R.-M. Nicoud, J. Chromatogr. A 702 (1995) 97.
[14] E. Dieterich, G. Sorescu, G. Eigenberger, Chem. Ing. Tech. 64 (1992) 136.
[15] B.A. Finlayson, Nonlinear Analysis in Chemical Engineering, McGraw-Hill, New York, 1980.
[16] P. Deckert, Ph.D. thesis, TU-Berlin, 1997
[17] C.B. Ching, K.H. Chu, K. Hidajat, M.S. Uddin, AIChE J. 38 (1992) 1744.
[18] J.B. Butt, Reaction Kinetics and Reactor Design, Prentice-Hall, Englewood Cliffs, NJ, 1980.
[19] Verein Deutscher Ingenieure, VDI-Warmeatlas, Datasheets for Heat Transfer, 7th Edition, VDI, Düsseldorf, 1994.
[20] G. Storti, M. Mazzotti, M. Morbidelli, S. Carra, AIChE J. 39 (1993) 471.
[21] M. Mazzotti, G. Storti, M. Morbidelli, J. Chromatogr. A 769 (1997) 3.
[22] H.-K. Rhee, R. Aris, N.R. Amundson, First-Order Partial Differential Equations, Vols. I and II, Prentice-Hall, Englewood Cliffs, NJ, 1986.
[23] F.G. Helfferich, G. Klein, Multicomponent Chromatography, Marcel Dekker, New York, 1970.
[24] D. Tondeur, M. Bailly, in: R.M. Nicoud (Ed.), Simulated Moving Bed: Basics and Applications, INPL, Nancy, 1993, p. 95.